JOURNAL OF PROPULSION AND POWER
Vol. 25, No. 6, November–December 2009

Air–Hydrogen Heat Exchangers for Advanced Space Launchers

Patrick Hendrick,* Nicolas Heintz,† and Didier Bizzarri†
Free University of Brussels, 1050 Brussels, Belgium
Francisco Romera‡
IberEspacio, 28010 Madrid, Spain
James Murray§
Techspace Aero, 4041 Milmort, Belgium
and
Philippe Ngendakumana¶
University of Liège, 4000 Liège, Belgium

DOI: 10.2514/1.41780

This paper deals with air–hydrogen heat exchangers intended to provide in-flight oxygen collection capability to a reusable or semireusable two-stages-to-orbit launcher with an oxygen collection phase in supersonic cruise at Mach 2.5. It aims to present a theoretical but mainly technological and experimental feasibility study of heat exchangers sufficiently efficient and reliable to suit the extreme requirements of this application. Two precoolers of two different types (shell and tubes, and plate and fins) have been selected and designed with the objective of fulfilling all constraints of the concept in terms of performance, leak tightness, reliability, compactness, etc. This design process has been validated with four subscaled breadboards (two of each type) tested on two test benches (for performance and leak tightness), developed by Belgium and Spain, in on-design and off-design conditions. All these results highlight the suitability of the new technologies given the extreme requirements of the concept. An optimum design for each technology is recommended considering its proper advantages and disadvantages. An innovative precooler technology is presented and tested.

Nomenclature

A	=	surface, m^2
A_{sf}	=	fin cross section, m^2
AU	=	global heat transfer coefficient, W/K
C	=	fluid velocity, m/s
$\dot{C}$	=	capacitive flow rate, $Q.c_p$, W/K
Cr	=	capacitive flow rate, $(Q.c_p)_{min}/(Q.c_p)_{max}$
Cv	=	flow coefficient of a valve
c_p	=	specific heat at constant pressure, J/kg · K
D_{curv}	=	diameter of curvature, m
D_{hyd}	=	hydraulic diameter, m
Di	=	inside diameter, m
D_p	=	depth, m
d	=	outside diameter, m
e	=	thickness, m
f	=	friction factor
h	=	convective heat transfer coefficient, W/m^2K
h_f	=	fin height, m
K	=	charge loss coefficient
Kc	=	contraction coefficient
Ke	=	expansion coefficient
k	=	conductivity, W/mK
L_p	=	passage length, m
l	=	length of tube, m
Nu	=	Nusselt number
n	=	number of passes
P	=	pressure, Pa
P_f	=	perimeter of a fin, m
Pr	=	Prandtl number
Q	=	mass flow rate, kg/s
Re	=	Reynolds number
R_{th}	=	thermal resistance, K/W
T	=	temperature, K
U	=	global heat transfer coefficient, W/Km^2
xd	=	diagonal pitch coefficient
xl	=	longitudinal pitch coefficient
xt	=	transversal pitch coefficient
ΔP	=	pressure drop, Pa
ε	=	effectiveness, %
ρ	=	density, kg/m^3
σ	=	ratio of the finned surface and the total transfer surface
ϕ	=	contraction ratio

Subscripts

acc	=	acceleration part
atm	=	atmospheric
c	=	cold side
D	=	diameter
f	=	fin
$f,0$	=	finned surface
h	=	hot side
i	=	inlet
max	=	maximum
min	=	minimum
o	=	outlet
p	=	pass

Received 24 October 2008; revision received 5 June 2009; accepted for publication 13 July 2009.

*Professor, Aerothermomechanics Department. Senior Member AIAA.
†Research Engineer, Aerothermomechanics Department.
‡Research Engineer.
§Head of Advanced Space Projects, Safran Group. Member AIAA.
¶Professor, Department of Aerospace and Mechanical Engineering.

I. Introduction

IN MOST of the past and current space launchers, a large and unused quantity of energy is generally stored in the liquid hydrogen present onboard as a fuel. In the 1950s, a first application was proposed to recover a part of this energy with the liquefied air cycle

engine. In this cycle, the air was deeply cooled by using the hydrogen before entering, mixed with H_2 fuel, into the combustor [1,2].

A possible improvement of this system would be to use the hydrogen to also cool down the air but, this time, to allow the separation of nitrogen and oxygen to get liquid oxygen (LOX) (or liquid air enriched in oxygen) for later use in rocket mode with an in-flight oxygen collection system also referred to in the U.S. literature as air collection and enrichment system (ACES) [2–4]. The main advantages of such systems are to present largely reduced takeoff gross weight and dry mass compared with current space launchers, to allow the construction of reusable launchers and to be compatible with different types of launchers [2,5].

To prove the feasibility of such an innovative reusable TSTO (two-stages-to-orbit) launcher concept, two main technologies must be proven. The first one is the air separator [6–8] used to split nitrogen and oxygen to store the air enriched in oxygen in the upper stage LOX tank (for later use in the upper liquid rocket engine). The second technology is the air–hydrogen precooler installed in the reusable first stage and used to deeply cool the air before the inlet of the air separator [2]. This paper will present a feasibility study of such advanced heat exchangers (HEX) used as precoolers. It will present innovative prototypes that were built and tested as well as models to size them and to calculate their performance and pressure losses.

II. System Definition and Specifications

The aim of this study was to evaluate the opportunities of in-flight LOX collection with an air collection and enrichment system applied to a fully reusable or semireusable supersonic TSTO launcher. The concept is to separate the atmospheric air into nitrogen and oxygen (the air being previously cooled with cold gaseous hydrogen) thanks to a rotary distillation unit [5–9]. The principle of this system is illustrated in Fig. 1.

As the LOX collection system requires an air intake, a compressor to compensate for the pressure drops, and an air (without much oxygen) exhaust, it was decided to put the ACES system in the secondary flow (bypass) of the propulsion system [5,10].

This paper will only focus on the front heat exchanger, also called the precooler.

The position of the system in the secondary flow of the gas turbine engine implies that the available place for the precooler is an annular space, as the secondary air crosses the precooler while the primary air flows into the engine. Figure 2 illustrates this configuration, presenting the details of the engine of Fig. 1.

This available annular space also imposes some of the geometric parameters of the precooler. In our design, the internal and external diameters are 1.48 m and 2.04 m, respectively, while the maximum allowed depth is 0.7 m. These geometric considerations are illustrated in Fig. 3, which presents the dimensions of the precooler shown in Fig. 2.

In terms of fluids, the coolant will be the hydrogen present onboard as a fuel. As hydrogen is stored in its parastate and as the conversion rate to orthohydrogen is lower than 1% per hour, the cold inlet of the precooler will receive gaseous parahydrogen at 200 K and 16 bar. This use of hydrogen implies a very high level of tightness between the two sides of the precooler to avoid accidents stemming from the mixing of hydrogen and air. The "hot fluid" will be, as stated earlier, air coming from the secondary (bypass) flow of the propulsion system. With these considerations, the system can be simulated and some results are shown in Fig. 4 [10].

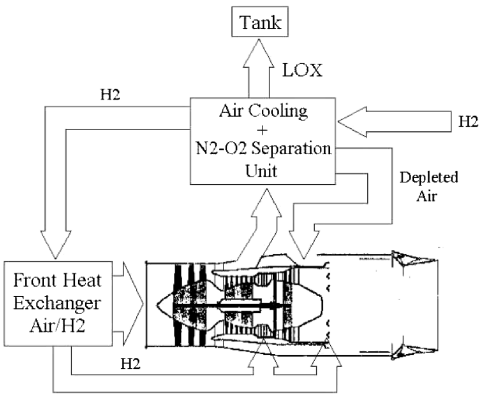

Fig. 1 Principle of the supersonic ACES.

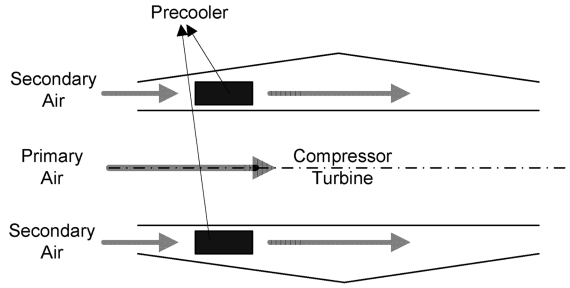

Fig. 2 Axial section of the engine and position of the precooler.

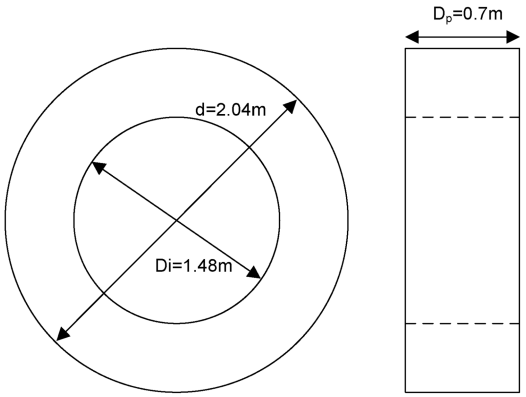

Fig. 3 Available annular space for the air-GH_2 precooler.

From this figure, it can be concluded that the precooler has to be resistant to extreme temperatures (from 208 K up to 480 K) and pressure resistant up to 16 bars on the cold side. The working values also imply a high effectiveness (about 90%, what will require several passes) and to dissipate a high thermal power (about 10.5 MW).

To be a useful technology, this system also has to be lighter than conventional systems. Combined with the upper remarks on effectiveness and available space, it can be concluded that the precooler must also have a high compactness.

Finally, the allowed pressure drops have to be very low, especially on the hot air side (only 0.15 bar vs 4 bar on the cold hydrogen side).

The philosophy followed in the framework of this study has been to size two separate precoolers according to the upper criteria and to prove the design process by testing four breadboards (BB) representative of the full precooler. The same framework will be followed in this paper which will present the sizing of the precoolers, the downscaling of these to create the breadboards, the test benches used for the tests, and their main results and conclusions.

III. Theoretical Study of the Precooler

As explained in the system definition, the main characteristics expected from the full-size precooler are as follows: to be pressure resistant up to 16 bar on the cold side, temperature resistant from 208 K up to 480 K, cost effective, light, to have a high compactness, a high effectiveness, to fit into the annulus space available in the launcher, and to show absolutely no mixing between the fluids. From those constraints, a choice had to be made between all types of heat exchangers existing on the market (recalled in Fig. 5 [11]).

Regenerators use a matrix which is crossed alternatively by the hot and the cold fluid. This changing of crossing could generate a mixing between the two fluids, which is strongly forbidden in the application. This technology has thus been rejected [11–13].

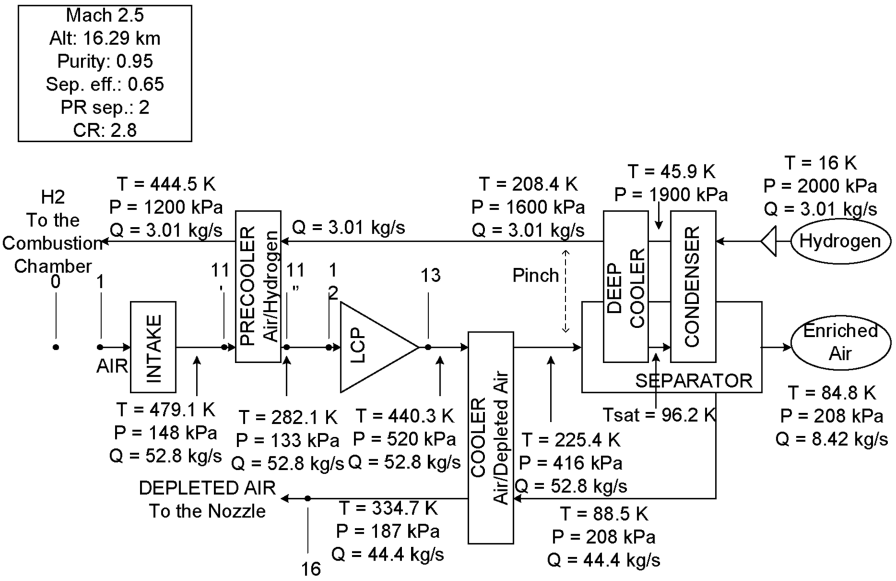

Fig. 4 Example of simulations of the ACES system.

The tubular HEX are made up of a set of tubes which contain the two fluids. This configuration is the most used and the most flexible regarding materials, fluids, and thermal duty. It thus presents an interesting topic to be investigated within this study and especially the shell-and-tubes (S&T) subtype which is more economically suitable for the studied application. This subtype has therefore been selected [11–13].

The plate-type HEX (PHE) are made up of thin plates between which fluids circulate. Printed-circuit PHE are made up of plates with microchannels bonded together to create a block. They generally create very high pressure drops and have therefore been rejected. Gasketed PHE are made with flat plates using elastomeric sealants to ensure the tightness between the fluids. As those sealants have a very limited temperature range (−40 to 260 °C), this subtype has been rejected. The spiral PHE are made up of two long metal sheets wrapped helically around a mandrel between which the fluids circulate. Because of the complexity of the configuration, leakages can appear at the junctions of the plates and at the manifolds. This configuration has therefore also been rejected. The other types of PHE, using welding or brazing, are not sensitive to those topics but, as their effectiveness can be strongly increased by adding fins between the plates (extended surface HEX), these configurations have not been investigated further within this study [11–13].

The extended surface heat exchangers are using fins between plates [plate and fins (P&F)] or around tubes (tubes and fins) to increase their effectiveness. These configurations fulfill all the requirements previously expressed with their high compactness, their high effectiveness, their manufacturability in aluminum alloys compatible with the pressure and temperature ranges, their low sensitivity to leakage, and their low pressure drops. As they do not require tubes which could be difficult to manufacture and assemble due to the small diameters required, plate-and-fins heat exchangers have therefore been preferred to the tube-and-fins HEX [11–13].

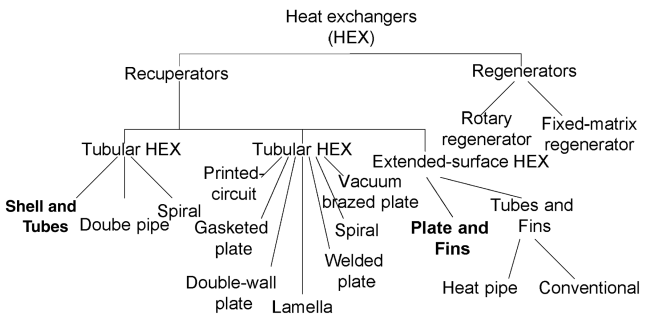

Fig. 5 Types of heat exchangers. (From Shah and Sekulic [11]; reprinted with permission.)

In conclusion, two models of heat exchangers have been selected to be studied within this study: the shell and tubes and the plate and fins.

The first kind that has been chosen is the shell and tubes, which is certainly the most used type of HEX, as well as the best known and the most versatile, as it can be adapted to any configuration in terms of geometry, pressure, and temperature. This configuration shows a low compactness (contact m^2/m^3) and a high effectiveness. However, some leakages from one side to the other can take place, even just after the manufacturing [13]. The experimental part of the study had as a fundamental objective of establishing the possibility of assuring the leak tightness with this configuration.

For the precooler, bare tubes have been selected rather than finned tubes, which are sensitive to air fouling and difficult to integrate into the launch vehicle. Furthermore, the use of fins reduces the number of tubes, increases the H_2 mass flow rate and increases the pressure drops on the cold side, which are a critical parameter for the ACES launcher application [14].

To size the full-size precooler, a parametric study has been performed to evaluate the influence of three geometric variables: the number of passes, the tube pitches (space between tubes), and the diameter of the tubes. This analysis has been performed with a constant wall thickness of the tubes of 0.25 mm. This value has been considered as optimal as it is the smallest value compatible with the application in terms of manufacturability and mechanical resistance. The other geometric parameters were imposed by the available space for integration into the launcher.

First, increasing the number of passes tends to decrease the matrix volume and mass, but only asymptotically. Moreover, the precooler becomes wider, shorter, and more complex mechanically, which limits the number of passes. An optimum of four passes has been found.

Second, the tube pitches coefficients (longitudinal xl, transversal xt, and diagonal xd) illustrated in Fig. 6 influence conversely the mass and the dimensions of the precooler. A compromise for the ratio xt/xd that minimizes mass, width, and height would be 1.7. An absolute value of xl, xt, and xd was then found according to the manufacturing constraints. An optimum with $xt = 2$ and $xl = 1.25$ has been chosen.

Third, when the tube inside diameter decreases, the tube mass and the matrix volume decrease too. Effectively, the height and the depth decrease linearly when the width increases exponentially, as the pressure drops have to be kept constant during the dimensioning. Effectively, as they are proportional to $(1/Di)^5$, the length of the tube had to be reduced exponentially and then the width increased

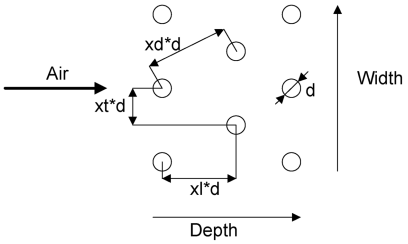

Fig. 6 Tube pitches coefficient for shell-and-tubes configuration.

exponentially. But the higher transfer coefficients in smaller tubes limit the augmentation of the number of tubes with the consequence that the global volume decreases linearly. The chosen value of the outside diameter for the tubes of the precooler was 3 mm. Table 1 summarizes the geometric parameters selected for the precooler.

The second HEX that was selected is a plate and fins because these heat exchangers have a high effectiveness and a high compactness [11–13]. Special attention had to be paid during the experimental part to the tightness of all connections to assure the reliability of this configuration for the air-GH_2 precooler.

As the external dimensions are fixed (as for the shell-and-tubes precooler) by the available annulus space, the only available dimensioning parameters are the types and the dimensions of the fins and the number of modules and passes.

For the fins, the choice had to be made within the catalogues of the manufacturers. The two most common types of fins are plain fins with no interruptions in the flow direction and fins with interruption in the flow direction.

In the first category, we have not only straight fins but also wavy fins, which present a "zigzag path" for the flow, which confers a higher convective heat transfer coefficient and a higher transfer surface but a higher friction factor (and therefore higher pressure drops) [13,15]. The second category includes louvered fins (triangle plain fins with "cuts" called louvers) and the offset strip fins (rectangular section divided in strips). These fins generally have a higher friction factor and transfer coefficient than plain fins. Figure 7 [16] and Fig. 8 [16] illustrate the different types of fins.

On the hydrogen side, where the pressure drop criteria is not so critical, offset strip fins have been selected for their higher transfer coefficient compared to plain fins and their better mechanical resistance compared to louvered fins [15]. In contrast, on the air side, where the pressure drops are really critical, plain fins have been selected. The simulations showed that the requirements of the application can be reached with both types of fins proposed by the manufacturers for the air side (straight plain fins or wavy plain fins) if the number of modules is adjusted to meet the air pressure drops expectations. Two plate-and-fins precoolers have therefore been designed in collaboration with two different manufacturers.

The first plate-and-fins precooler has offset strip fins at the hydrogen side and straight plain fins at the air side. Two models of offset strip fins were proposed by the first manufacturer for the hydrogen side: one with higher fins but more spaced than the other. The densest model allows keeping a high convective transfer coefficient with a better mechanical resistance but with higher pressure drops. But, as these are not so critical on the hydrogen side, this type of fin has been selected. These fins have a height of 1.76 mm, a length of 3 mm, and are spaced by 1.293 mm for a global density of 17.6 fins per inch. On the air side, both wavy and straight plain fins were possible but, as the second manufacturer only proposed wavy fins, straight fins have been selected on the first precooler to perform a

Table 1 Optimum geometric dimensions of the shell-and-tubes precooler

Outside tube diameter	3 mm
Tube thickness	0.25 mm
Number of passes	4
Tube pitch	$xt = 2; xl = 1.25$

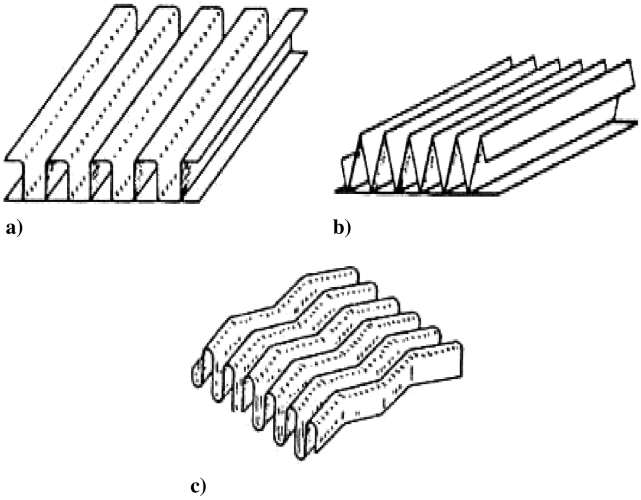

Fig. 7 Fins with no interruption in the flow direction: a) rectangular, b) triangular, c) wavy. (From Bontemps et al. [16]; reprinted with permission.)

comparison of these two types of fins. For the straight fins, four models were available with variable heights. As on the air side, where the pressure drops are critical, a tradeoff had to be made between the thermal performance requiring the highest fins possible and the pressure drop requiring the smallest fins possible. An intermediate value has therefore been selected with fins having a height of 7.85 mm spaced by 1.389 mm for a density of 16.5 fins per inch.

The second plate-and-fins precooler was built by another manufacturer who only proposed one type of fin for each side of the precooler: offset strip fins of 2.35 mm height, 2.04 mm length, and spaced at 0.85 mm on the hydrogen side, and wavy fins of 11.6 mm height, spaced at 1.44 mm with a distance between two maximums of a wave of 9.6 mm, and a radius of curvature of 3 mm.

Both plate-and-fins precoolers have three passes of hydrogen and one pass of air.

For the material, three materials are suitable for heat exchangers: titanium alloys, stainless steels, and aluminum alloys. First, the titanium was rejected because of risks of embrittlement by hydrogen penetration. Second, stainless steels could be a solution but they are, depending on the type of steel, either prone to cold cracking (martensitic steels) or suitable to hydrogen embrittlement and hard to weld (ferritic steels) so that only austenitic stainless steels could have fit the application requirements (i.e., AISI TP316L). The third option was aluminum alloys, which give the best results in terms of mass (lowest density) and thermomechanical performance. The disadvantages of aluminum alloys are their low stress resistance, especially at high temperature (here 480 K) and their low corrosion resistance. However, some aluminum alloys series meet the requirements of the project, such as the 3xxx (Al-Mn), 6xxx (Al-Mg-Si), and the 7xxx (Al-Zn) series. For the precooler, aluminum alloys were finally chosen. The selected aluminum alloy type will depend on the HEX configuration [17,18].

The performances of all the precoolers detailed earlier have been simulated using the ε-NTU method, which predicts the effectiveness of a heat exchanger as a function of a dimensionless number defined as $\mathrm{NTU} = AU/\dot{C}_{\min}$.

For the shell and tubes heat exchanger, the global heat transfer coefficient has been defined as the product of the surface of exchange and the conductivity associated with this surface, which is defined for cylindrical tubes without fins as

$$U = \left[\frac{d}{Dih_c} + \frac{d}{2k}\ln\left(\frac{d}{Di}\right) + \frac{1}{h_h}\right]^{-1}$$

In this formula, the convective heat transfer coefficients can be estimated by the following relations:

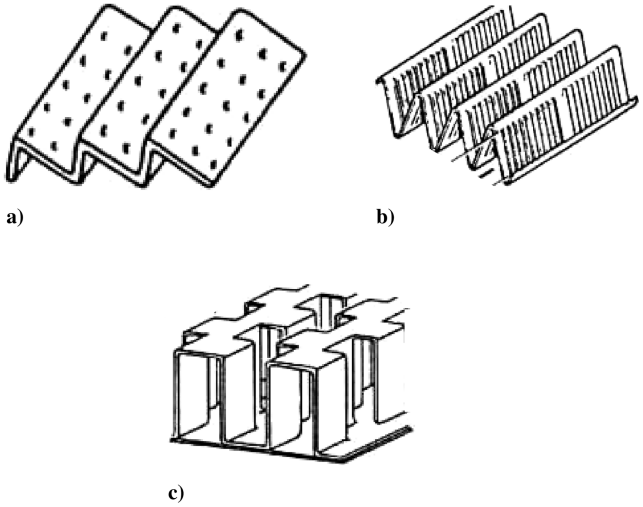

Fig. 8 Fins with interruption in the flow direction: a) perforated, b) louvered, c) offset. (From Bontemps et al. [16]; reprinted with permission.)

1) At the cold side,

$$h_c = \frac{k_c}{Di} 0.023 Re_c^{0.8} Pr_c^{0.4}$$

is valid for Reynolds numbers from 3.10^4 to 10^6 [19].

2) At the hot side,

$$h_h = \frac{k_h}{d} 0.41 Re_h^{0.6} Pr_h^{0.33} \left(\frac{xt}{xl}\right)^{0.16667}$$

is valid if $xt/xl < 2$ [14].

For the plate-and-fins heat exchanger, the global heat transfer coefficient is defined as the inverse of the total thermal resistance, which has three major components that must be summed: the resistance of the fins at the air side, the resistance of the fins at the hydrogen side, and the resistance of the wall. For the fins, these resistances can be calculated by using the following procedure:

$$m_f = \left[h \frac{P_f}{k_{\text{wall}} A_{\text{sf}}}\right]^{0.5} \rightarrow \varepsilon_f = \frac{\tanh\left(m_f \frac{h_f}{2}\right)}{m_f \frac{h_f}{2}} \rightarrow \varepsilon_{f,0} = 1 - \phi(1 - \varepsilon_f)$$
$$\rightarrow R_{\text{th}} = \frac{1}{\varepsilon_{f,0} \cdot h \cdot A} \tag{1}$$

The convective heat transfer coefficients for the fins are calculated by the knowledge of the Nusselt numbers ($Nu = h \cdot D_{\text{hyd}}/k$) estimated with the following correlations:

1) For offset strip fins, the correlations (accuracy 20%) of Manglik and Bergles have been used [20]:

$$f_{\text{offset}} = 38.4972\, Re_D^{-0.7422}\, \alpha^{-0.1856}\, \delta^{0.3053}\, \gamma^{-0.2659} \times [1 + 7.66910^{-8} \quad Re_D^{4.429} \quad \alpha^{0.92} \quad \delta^{3.767} \quad \gamma^{0.236}]^{0.1} \tag{2}$$

$$Nu = 0.6522\, Re_D^{0.4597}\, Pr^{1/3}\, \alpha^{-0.1541}\, \delta^{0.1499}\, \gamma^{-0.0678} \times [1 + 0.00005269 \quad Re_D^{1.34} \quad \alpha^{0.504} \quad \delta^{0.456} \quad \gamma^{-1.055}]^{0.1} \tag{3}$$

In those formulas, α, δ, and γ are defined as the ratios, respectively, between the internal width and the internal height of the fins, the thickness and the length of the fins, and the thickness and the internal width of the fins.

2)For the straight plain fins, the Filolenko's correlations [21] (valid for $Re > 5000$) and Gnielinski's correlation [11] (valid for Re from 2300 to $5 \cdot 10^6$ and for Pr from 0.5 to 200) have been used:

$$f_{\text{plain}} = (1.82 \cdot \log_{10}(Re) - 1.64)^{(-2)} \tag{4}$$

$$Nu = \frac{\frac{f}{8}(Re - 1000) \cdot Pr}{1 + 12.7[\frac{f}{8}]^{0.5}(Pr^{\frac{2}{3}} - 1)} \tag{5}$$

3) For the wavy fins, graphical correlations that can be found in [15] have been considered.

All these formulas are valid for straight fins, which is not representative of the situation in the precooler. As a consequence, those correlations have been corrected to take into account the radius of curvature of the precooler:

$$f_{\text{curved}} = f_{\text{straight}} + 0.03 \cdot \sqrt{D_{\text{hyd}}/D_{\text{curv}}} \tag{6}$$

For the wall, the thermal resistance can be calculated with the formula $R_{\text{th}} = e/(k \cdot A)$.

The knowledge of the NTU parameter allows the calculation of the effectiveness of the heat exchanger while using the formulas presented in Table 2 [11].

For the shell and tubes unit, a counterflow configuration has been considered for the global heat exchanger and a crossflow configuration ($\dot{C}_{\text{min}}$ unmixed) has been considered for single pass.

For the plate-and-fins precoolers, each pass has been considered as a purely crossflow configuration (with both fluids unmixed) connected together with accurate boundary conditions to obtain the full-size precooler.

To estimate the pressure drops, three contributions have been considered: the pressure drop due to friction along channels, the pressure drop due to contraction and expansion at the inlet and the outlet of the precooler, and the pressure drop due to the acceleration at the inlet of the channels. The largest part of the pressure drops comes from the friction.

For the shell and tubes unit, the pressure drops are estimated to be

$$\Delta P_h = \frac{K}{2\rho_h} \left(\frac{Q_{h,\text{in}}}{A_{\text{free}}}\right)^2 \tag{7}$$

$$\Delta P_c = \frac{fl}{d} \frac{1}{2\rho_c} \left(\frac{Q_{c,\text{in}}}{n\pi Di^2/4}\right)^2 \tag{8}$$

For the plate-and-fins units, the pressure drops are estimated to be the sum of the following components:

$$\Delta p_{\text{friction}} = \frac{1}{2} \cdot f \cdot \rho \cdot \frac{L_p}{D_{\text{hyd}}} \cdot C^2 \tag{9}$$

Table 2 Relations ε-NTU

Flow configuration	Relations ε-NTU
Counterflow	$\varepsilon = \frac{1-e^{-\text{NTU}(1-C_r)}}{1-C_r e^{-\text{NTU}(1-C_r)}}$
Crossflow	$\varepsilon = 1 - e^{\frac{\left(e^{-\text{NTU}^{0.78} C_r} - 1\right)\text{NTU}^{0.22}}{C_r}}$
Parallel flow	$\varepsilon = \frac{1-e^{-\text{NTU}(1+C_r)}}{1+C_r}$
Crossflow, $\dot{C}_{\text{min}}$ unmixed	$\varepsilon = \frac{1}{C_r}\left[1 - e^{-C_r\left(1-e^{-\text{NTU}}\right)}\right]$
Crossflow, $\dot{C}_{\text{max}}$ unmixed	$\varepsilon = 1 - e^{-\frac{1}{C_r}\left(1-e^{-\text{NTU}.C_r}\right)}$
Multipass overall counterflow (fluid mixed between passes)	$\varepsilon = \frac{\left(\frac{1-\varepsilon_p C_r}{1-\varepsilon_p}\right)^n - 1}{\left(\frac{1-\varepsilon_p C_r}{1-\varepsilon_p}\right)^n - C_r}$
Multipass overall parallel flow (fluid mixed between passes)	$\varepsilon = \frac{1}{1+C_r}[1 - \{1 - (1 + C_r)\varepsilon_p\}^n]$
All configurations, $C_r = 0$	$\varepsilon = 1 - e^{-\text{NTU}}$

Table 3 Precooler conditions and expected performance

	S&T	First P&F	Second P&F
Q_c, kg/s	3.01	3.01	3.01
Q_h, kg/s	52.8	52.8	52.8
$T_{c,i}$, K	208.4	208.4	208.4
$T_{h,i}$, K	479.1	479.1	479.1
$P_{c,i}$, bar	16.0	16.0	16.0
Δp_c, bar	4.02	2.86	2.55
$P_{h,i}$, bar	1.48	1.48	1.48
Δp_h, bar	0.15	0.145	0.37
$Re_{c,i}$	24,115	7912	5295
$Re_{h,i}$	5022	6108	6071
Compactness, m^2/m^3	418.2	1549	1639
ε, %	86.72	87.88	90.58

$$\Delta p_i = \frac{(\rho \cdot C)^2}{2 \cdot \rho_i} \cdot (Kc + 1 - \sigma^2) \tag{10}$$

$$\Delta p_o = -\frac{(\rho \cdot C)^2}{2 \cdot \rho_o} \cdot (1 - Ke - \sigma^2) \tag{11}$$

$$\Delta p_{\text{acc}} = (\rho \cdot C)^2 \cdot \left(\frac{1}{\rho_o} - \frac{1}{\rho_i}\right) \tag{12}$$

In these formulas, the coefficients Ke and Kc can be found in the literature [15] and the friction factors f of the different fins are those described previously.

From those simulations, the expected design-point conditions and performances of the air-GH_2 precoolers have been calculated and are shown in Table 3.

IV. Test Facilities

A. Scaling of the Precooler and Test Conditions

The tests that had to be performed in the framework of this study had two major objectives: to test the performance (mainly the HEX effectiveness and the pressure drops on both sides) of breadboards representative of the full-size precooler to validate the correlations used during the dimensioning and to test the leak tightness of these breadboards after some thermomechanical fatigue cycles to prove the reliability of the selected technologies for the ACES launcher application.

To realize the performance tests, two types of adaptations had to be made to allow the testing in a laboratory environment: adaptations of the test conditions and adaptations of the heat exchangers to create four breadboards representative of the full-size precooler.

Table 4 HEX testing conditions

	S&T BB	First P&F BB	Second P&F BB
Q_c, g/s	100	400	180
Q_h, g/s	500	500	440
$T_{c,i}$, K	280	280	280
$T_{h,i}$, K	390	470	470
$P_{c,i}$, bar	3	3	4.7
$P_{h,i}$, bar	$P_{\text{atm}} + \Delta P$	$P_{\text{atm}} + \Delta P$	$P_{\text{atm}} + \Delta P$
$Re_{c,i}$	23,464	8100	5430
$Re_{h,i}$	5471	6300	5400

The main modifications of the flow conditions were the limitations of the cold inlet pressure at 3 bar and of the hot mass flow rate at 500 g/s to limit the electrical power required to heat up the air. From these modifications and in light of the replacement of hydrogen by air as the cold fluid for safety reasons, the cold flow has been calculated to keep the same capacitive flow rates $((Qc_p)_{\min}/(Qc_p)_{\max})$ as in the precooler. This reduced cold flow rate also allows the cooling of this flow to lower temperatures (lower than 0 °C) with a rather small flow of liquid nitrogen (in Fig. 9, cold temperature regulation). Moreover, the temperature has been chosen to reach the maximal temperature gradient present in the precooler to verify that no metal expansion problem occurs in these extreme cases. A summary of the test conditions of the breadboards is shown in Table 4. With these adaptations of the flow conditions, the geometry of the heat exchangers has to be scaled down and adapted to be representative of the full-size precooler.

As the thermal effectiveness per fluid pass had to be conserved, the numbers of heat transfer units have been adapted. Furthermore, the frontal sections of the breadboards have been calculated to keep the Reynolds number constant and then the "global flow conditions" equal to the ones of the precooler. By contrast, no modifications were required to keep the Prandtl number constant in the breadboards as we keep a gas-to-gas heat exchanger.

In a more manufacturing-type approach, the breadboards have been designed flat instead of curved as the high required radius of curvature (0.88 m) produces limited modifications to the performance and introduces major manufacturing problems. Except for this, all the other manufacturing characteristics (materials, fins, tubes, assembly methods) have been kept identical.

B. Performance Test Bench

To establish the performance of the breadboards and realize the required thermomechanical fatigue cycling, a first test bench has been built. The principle of this performance test bench is shown in

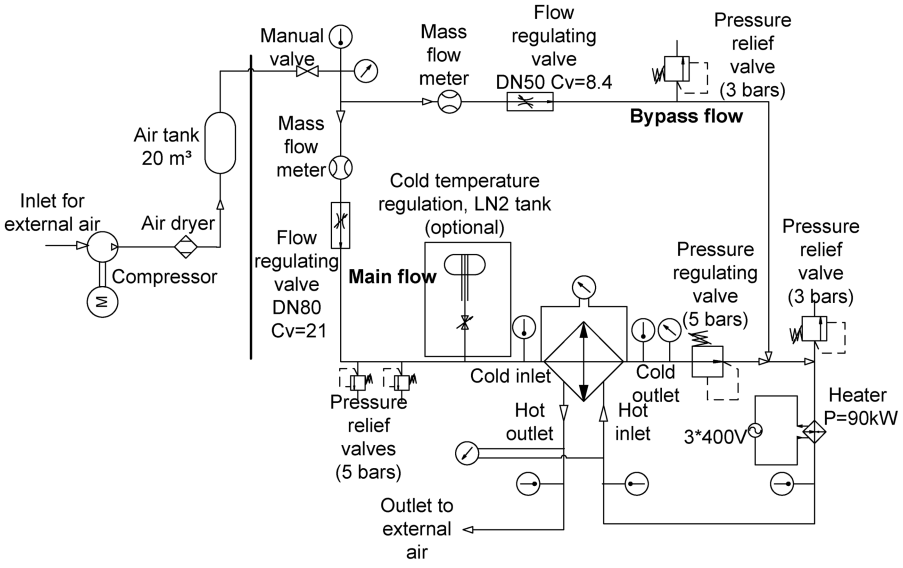

Fig. 9 Performance test bench schematic.

Fig. 9. The elements that can be seen in Fig. 9 are from the inlet to the outlet:

1) The generation and the storage of dry compressed air at 40 bar is realized with a two-stage piston compressor, a dryer, and a 20 m^3 air tank. A manual valve has been added at the outlet of the tank to have a "blown-down facility" which serves to fill the tank using the compressor and then to empty the tank in the test bench with the compressor off.

2) A first line called "cold flow" brings the air to the cold inlet of the breadboard to be tested. This line includes a mass flow meter, a mass flow regulating valve, a pressure regulating valve, several temperature sensors to evaluate the effectiveness of the HEX, several relative pressure sensors to regulate the pressure and to monitor the test bench for the safety of the operators, a differential pressure sensor to measure the pressure drops along the HEX, two pressure relief valves, and a liquid nitrogen tank to add some liquid nitrogen to the flow to decrease the cold inlet temperature for some tests.

3) A second line called "bypass flow" allows the increase of the mass flow between the cold side and the hot side of the HEX. It includes the same flow regulating system as in the cold line.

4) The mixing of the two flows gives the hot flow which is heated up into an electrical heater of 100 kW to reach the hot inlet of the HEX. Several temperature sensors and a differential pressure sensor are also present to evaluate the performance of the breadboard.

A picture of this test bench is shown in Fig. 10, with some indications of the different flows.

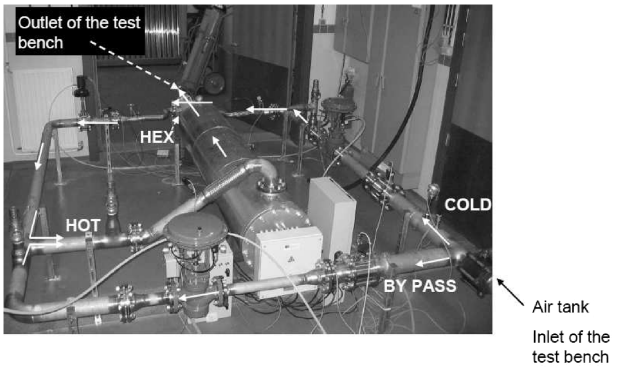

Fig. 10 Performance test bench.

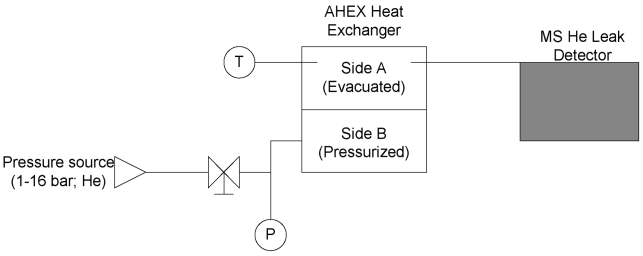

Fig. 11 Helium vacuum leak detection test principle.

C. Leak Detection Test Bench

To test the leak tightness of the breadboard, the helium vacuum detection method has been used. It consists of pressurizing (at about 1 bar) one side of the heat exchanger with helium and depressurizing the other side to a vacuum pressure of about 10^{-2} mbar, where the concentration of helium is then monitored. To do this monitoring, a leak detector that is able, according to the manufacturer's data,** to measure a leak from 10^{-12} mbar $\cdot$ l/s to 1 mbar $\cdot$ l/s has been employed. A schematic of the principle is shown in Fig. 11.

For these tests, an upper limit for the detected helium leak flow of $5.06 \cdot 10^{-4}$ mbar $\cdot$ l/s or $5 \cdot 10^{-4}$ sccs (0.1 μg/s of helium or 0.05 μg/s of hydrogen) has been fixed. This value can be understood as the addition of the maximum leaks (10^{-6} mbar $\cdot$ l/s) of about 1000 metallic joints (equivalent to one heat exchanger). It should be noted that this value is extremely restrictive (less than 0.1 μg/s of gaseous hydrogen to be compared with the hundreds of grams per second that pass into the breadboards in real use), so that this limit must be understood more as an objective or as an order of magnitude rather than a real maximum value.

V. Breadboards Performance and Leak Testing

As explained in the previous sections, the tests had as their main objectives to validate the performance (effectiveness and pressure drops) and the mechanical resistance (in terms of leak tightness) after several fatigue cycles of breadboards representative of the full-size precooler. The results should prove the validity of the simulations and estimations used to size the precooler and the compatibility of the selected technologies with the ACES launcher application requirements.

For the initially selected configuration (shell and tubes), two breadboards (one pass of each fluid) have been built with two different types of connections between the end plates and the tubes. All the other parameters were kept strictly identical. The two connection systems that have been tested are the ferruled connections and the brazed connections, as illustrated in Fig. 12. The aim of the construction of these two different breadboards was to compare the two assembly systems in terms of leak tightness and resistance to thermomechanical fatigue.

**SMARTTEST Helium Leak Detector HLT560 PTL0200, http://www.pfeiffer-vacuum.net.

For the second selected configuration (plate and fins), two breadboards have also been manufactured but with larger differences. The first demonstrator has one pass of cold fluid, straight plain fins at the hot side, and offset strip fins at the cold side. The second breadboard has two passes of cold fluid, wavy plain fins at the hot side, and offset strip fins at the cold side.

In terms of leak tightness, the two shell-and-tubes breadboards gave very small helium leak flows but, unfortunately, were over the

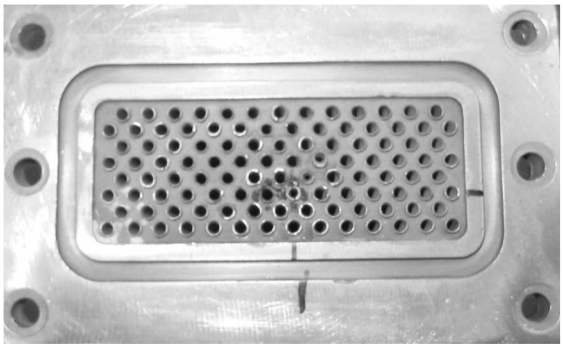

a)

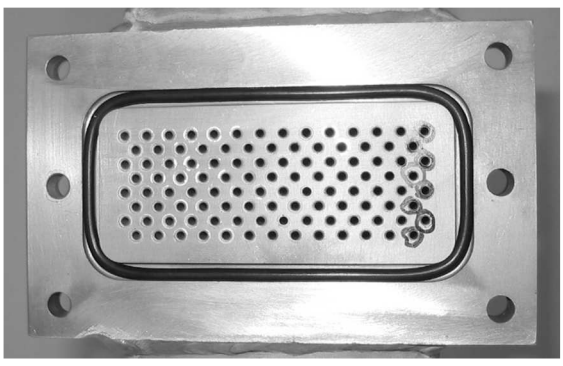

b)

Fig. 12 Tube end plate connections: a) brazed, b) ferruled.

specified limit. However, the leak flows were rather stable over time, indicating a good resistance to thermomechanical fatigue and as the leak flows were of the right order of magnitude. It can be concluded that the shell-and-tubes concept is a very promising technology. It could fulfill the ACES application requirements with an efficient leak acceptance test after the production of the unit and a follow-on inspection when in use on the reusable first stage of the space launcher.

Among other things, we compared the two assembly technologies. The brazed connections were a bit over the leak limit, apparently because of just one problematic connection. A repair of this leak could potentially solve the problem. However, this repair procedure has not been tested within this study and is not so easy to successfully perform. By contrast, all the ferruled connections showed a slightly excessive leak flow, and it is the addition of all these small flows that caused the test results to fall just over the limit. These results showed that the innovative concept of ferruled connections is now mature enough to allow very high-quality manufacturing and consistent quality of the connections. However, special attention must be paid to the manufacturing time as the ferruled connections are made one at a time, whereas the brazed connections are done all at once. These observations lead to the conclusion that, if a choice had to be made between the two connection systems, the ferruled one should be preferred as it is easier to repair than the brazed option, despite the higher manufacturing time.

By contrast, the plate-and-fins breadboards have passed all the helium leak detection tests with full success. A small increase of the global leak flow has been observed after several cycles of utilization, but it was always within the limits, so that this configuration is fully compatible with the launcher application requirements. All the results of the helium leak tests are presented in Table 5 (always with one leak test after three performance tests).

In terms of performance, a comparison (shown in Table 6) between the experimental and simulated results has been performed and validated the simulations in terms of exchanged power and then in terms of temperature differences and HEX effectiveness.

For the experimental results, no deterioration of performance has been observed over time so that the mean of all the results has been considered for each breadboard. Moreover, as the leakage on the brazed unit does not impact the performance and as both shell-and-tubes units are rigorously identical from a geometric point of view, the two units have been considered as one despite the fact that they have both been tested.

Table 5 HEX leak tests results

	Brazed S&T $*10^{-5}$ sccs	Ferruled S&T $*10^{-5}$ sccs	First P&F $*10^{-5}$ sccs	Second P&F, $*10^{-5}$ sccs
Test 1, acceptance	487	99	4.9	9.87
Test 2	265	93	12.8	16.78
Test 3	333	88	5.43	21.7
Test 4, final	335	103	0.8	26.7

Table 6 Comparison of the experimental and calculated results

	S&T		First P&F		Second P&F	
	Exp.	Sim.	Exp.	Sim.	Exp.	Sim.
ε, %	52.1	57.3	51.3	61.0	50.0	60.7
ΔP_c, mbar	43	215	357	411	499	1290
ΔP_h, mbar	14	19	46	136	21	85

Table 7 Comparison of the breadboards with respect to compactness

	S&T	First P&F	Second P&F
Compactness, m^2/m^3	385	1530	1593
Volumetric power, MW/m^3	6.57	9.06	1.67
Power per mass unit, kW/kg	28.65	18.13	4.34

For the simulated results, the ε-NTU method described previously has been used on the breadboard's geometry.

For the pressure drops shown in Table 6, it has been observed that the empiric relations found in the literature [14,15,20–24] tend to rather largely overestimate the pressure drops for all selected heat exchangers. Actually, these theoretical laws are based on experiments and the difference between the test conditions implies a rather large difference between the modeling and the real results. However, these variations lean in a favorable direction in the present study as it adds a design margin between the simulations and reality.

A comparison between the configurations in terms of compactness and power exchanged per volume and mass unit has been made and is shown in Table 7. In this table, it can be observed that despite their lower compactness, the shell-and-tubes breadboards exchanged more power per unit of volume and mass, a major advantage in this application. This is the main reason why the shell-and-tubes configuration has certainly not been rejected despite its relatively worse helium leak test results.

VI. Off-Design Tests

The use of the heat exchangers in off-design conditions does not imply any problem, as it has been observed that a modification of the Reynolds number at the inlets of the HEX does not modify significantly their effectiveness if the capacitive flow rate is kept constant. The pressure drops are of course related to the Reynolds number as they are related to the flow speed and Mach number. The theoretical law that predicts a square dependence between the two variables has been observed.

All four heat exchangers have also been tested at low inlet cold side temperatures (down to $-70\,^{\circ}C$) without any significant decrease of the effectiveness despite the formation of a little frost which, of course, implies an increase of the pressure drop at the cold side (about twice as high). The relative humidity of the air was similar to the one at the cruise altitude of 16.3 km.

During all these tests, the breadboards have been heated up and cooled down at the extreme temperatures at which the precooler should be used. No problems of material resistance have been observed, which confirms the compatibility of aluminum and of the two selected configurations within the space launcher application constraints. This rather extreme use of the HEX from a thermomechanical fatigue point of view is certainly a very interesting result of this study.

It can be concluded from all these results that the plate-and-fins technology should be preferred if safety is the first criteria, given its better results during the leak tests. If this configuration is selected, wavy plain fins with their higher heat transfer coefficient should certainly be chosen at the hot side without any prejudice to the pressure drop requirements. At the cold side, the offset strip fins can be chosen as they fulfill the ACES launcher application requirements. But, given their better results in terms of exchanged power per mass and volume unit, *the shell-and-tubes configuration is certainly the best choice*. Effectively, their leak tests results were of the right order of magnitude and, most importantly, their performance was superior. If this configuration is chosen, the ferrule technology should be preferred to connect the tubes to the end plates as it is easier to repair than the brazed option despite the longer manufacturing time.

VII. Conclusions

After the successful testing of our rotary distillation separator concept and prototype for enriching the air in oxygen for the second-stage liquid rocket engines of a reusable TSTO launcher collecting oxygen enriched air in cruise at Mach 2.5 [7,8], another challenge was the fabrication and testing of the adequate heat exchangers for the air precooling, which are located in front of the turbofan compressor and of the air separator. This experimental study has proven the feasibility of this air–hydrogen precooler, showing

virtually no leak (only about 0.1 μg/s of hydrogen) and high performance. Different heat exchanger prototypes were built, using different technologies, tested and compared, and models for the heat exchanger performance and pressures losses were established. Moreover, those heat exchangers have been built in a lightweight material and using currently available manufacturing techniques. They also show a high volumetric power. The recommended technology is a shell-and-tube aluminum precooler using ferruled connections between the tubes and the end plates.

The design tools to be used for the full-size precooler have also been experimentally validated, as well as the pressure losses correlations even with, in this case, some overestimations.

Acknowledgments

The authors would like to thank the European Space Agency and the Belgian Ministry of Scientific Policy for their support. They also wish to thank the numerous contributors from various companies who participated in the study.

References

[1] Qi, F., Wang, J., and Chen, C.-P., "Preliminary Analysis of an Air Breathing and Rocket Combined-Cycle Engine," *Journal of Propulsion and Power*, Vol. 14, No. 5, Sept.–Oct. 1998, pp. 613–619. doi:10.2514/2.5353

[2] Maurice, L., Leingang, J., and Carreiro, L., "Air breathing Space Boosters Using In-Flight Oxidizer Collection," *Journal of Propulsion and Power*, Vol. 12, No. 2, March–April 1996, pp. 315–321. doi:10.2514/3.24030

[3] Andrews, J., and Andrews, D., "Low Cost Options for 2nd and 3rd Generation Reusable Launch Vehicles," *36th Joint Propulsion Conference*, AIAA Paper 2000-3824, July 2000.

[4] Andrews, J., and Andrews, D., "Designing Reusable Launch Vehicles for Future Space Markets," *52nd International Astronautical Congress*, International Academy of Astronautics IAA-01-IAA.1.1.07, Oct. 2001.

[5] Hendrick, P., and Saint-Mard, M., "Sänger-Type TSTO Using In-Flight LOX Collection," *Joint Propulsion Conference*, AIAA Paper 97-2858, July 1997.

[6] Bizzarri, D., Hendrick, P., Heintz, N., and Ngendakumana, P., "Compact Air Separation Technology For In-Flight Oxygen Collection," AIAA Paper 2008-2501, April–May 2008.

[7] Bizzarri, D., Hendrick, P., and Heyen, G., "Analysis of Minimal In-Flight Oxygen Collection Cycle for 2-Stage Launcher," AIAA Paper 2006-8097, Nov. 2006.

[8] Bizzarri, D., Hendrick, P., Heyen, G., and Ngendakumana, P., "Propulsion Vehicle Integration for Reusable Launcher Using In-Flight Oxygen Collection," *Aerospace Science and Technology*, Vol. 12, No. 6, 2008, pp. 429–435. doi:10.1016/j.ast.2007.10.012

[9] Balepin, V., Hendrick, P., Pelloux-Gervais, P., and Saclier, F., "O_2/N_2 Separation Processes for LOX Collection with Air Breathing Propulsion Systems," *AAAF Space Launchers Symposium*, 24 May 1996.

[10] Marquet, B., Hendrick, P., Strengnart, M., and Breugelmans, F., "Fully and semi-reusable, T.S.T.O. using in-flight LOX collection," *3rd European Conference on Space Transportation Systems*, Association Aéronautique et Astronautique de France, AAAF-STS-99-102, Nov.–Dec. 1999.

[11] Shah, R. K., and Sekulic, D. P., *Fundamentals of Heat Exchanger Design*, Wiley, Hoboken, NJ, 2003.

[12] S. Kakaç, and Liu, H., *Heat Exchangers: Selection, Rating and Thermal Design*, CRC Press, Boca Raton, FL, 2003.

[13] Kuppan, T., *Heat Exchanger Design Handbook*, Marcel Dekker, New York, 2000.

[14] Idelchik, I. E., *Handbook of Hydraulic Resistance, Coefficients of Local Resistance and of Friction*, National Science Foundation, Washington, D.C., 1960 (Translation).

[15] Kays, W. M., and London, A. L., *Compact Heat Exchangers*, McGraw–Hill, New York, 1964.

[16] Bontemps, A., Garrigue, A., Goubier, C., Huetz, J., Marvillet, C., Mercier, P., and Vidil, R., Echangeurs de chaleur: Intensification des échanges, Techniques de l'ingénieur: traité de génie énergétique, 1994.

[17] ASME Standard, American Society of Mechanical Engineers, Fairfield, NJ, 1995.

[18] Inchaurza Zabala, A., *Aceros Inoxidables y Aceros Resistentes al Calor*, Limusa Wiley, New York, 1981.

[19] Babcock and Wilcox Co., *Steam, Its Generation and Use*, Kessinger, Whitefish, MT, 2005.

[20] Manglik, R. M., and Bergles, A. E., "Heat Transfer and Pressure Drop Correlations for the Rectangular Offset Strip Fin Compact Heat Exchanger," *Experimental Thermal and Fluid Science*, Vol. 10, No. 2, 1995, pp. 171–180. doi:10.1016/0894-1777(94)00096-Q

[21] Adams, T. M., Abdel-Khalik, S. I., Jeter, S. M., and Qureshi, Z. H., "An Experimental Investigation of Single-Phase Forced Convection in Microchannels," *International Journal of Heat and Mass Transfer*, Vol. 41, Nos. 6–7, March 1998, pp. 851–857. doi:10.1016/S0017-9310(97)00180-4

[22] Ito, H., "Friction Factors in Turbulent Flow in Curved Pipes," *Journal of Basic Engineering*, Vol. 81, No. 2, June 1959, pp. 123–134.

[23] Rohsenow, W. M., Hartnett, J. P., and Cho, Y. I., *Handbook of Heat Transfer*, 3rd ed., McGraw–Hill, New York, 1998.

[24] Rohsenow, W. M., and Hartnett, J. P., *Handbook of Heat Transfer*, McGraw–Hill, New York, 1973.

D. Talley
Associate Editor